Small-signal stability analysis for microgrids under uncertainty using Malann control technique

Venkatesan, Anantha Krishnan; Swathika, O. V.Gnana; Subramaniam, Umashankar; Bhaskar, Mahajan Sagar; Almakhles, Dhafer J.; Padmanaban, Sanjeevikumar; Mitolo, Massimo

Published in:
IEEE Systems Journal

DOI (link to publication from Publisher):
10.1109/JSYST.2020.3020509

Publication date:
2021

Document Version
Accepted author manuscript, peer reviewed version

Small-Signal Stability Analysis for Microgrids Under Uncertainty Using MALANN Control Technique

Anantha Krishnan Venkatesan, Umashankar Subramaniam, *Senior Member, IEEE*, Mahajan Sagar Bhaskar, *Senior Member, IEEE*, O. V. Gnana Swathika, *Senior Member, IEEE*, Sanjeevikumar Padmanaban, *Senior Member, IEEE*, Dhafer J. Almakhles, *Senior Member, IEEE*, and Massimo Mitolo, *Fellow, IEEE*

***Abstract*—Microgrids are often considered as the solution for affordable and clean energy in the distribution sector. This article presents the small-signal stability analysis of a distributed generation unit in an autonomous microgrid operation. The purpose of the proposed strategy is to optimally improve the capacity of the power system to restore the reasonable operating condition following a small physical disturbance. The proposed strategy is the joined execution of both the modified antlion optimization algorithm (MALO) and artificial neural network (ANN), and hence it is abbreviated to MALANN. In this article, the proposed controller comprises two control loops, namely the inner current control loop and the outer power control loop. The MALO technique is incorporated to generate the dataset of possible proportional integral (PI) gain parameters. By using the accomplished dataset of MALO, the ANN is trained, and convincing estimate execution is brought out through the entire machine working condition. The proposed strategy is implemented in MATLAB/Simulink, and the results are examined with two test cases and compared with various solution techniques such as base method and ant-lion optimization. The results prove that the stability analysis is reasonably accurate, and the controller offers a reliable system's operation.**

***Index Terms*—Artificial neural network (ANN), clean energy, climatic changes, distributed generation, inner current and outer power control loop, modified antlion optimization (MALO), small-signal stability analysis, sustainable communities, system state matrix.**

I. Introduction

DEVELOPING natural concerns and competitive energy policies have prompted the decentralization of power generation. They have in-turn facilitated in realizing sustainable communities in the distribution network. Installations of distributed generators (DGs), such as photovoltaic, wind, etc., are expected to increase worldwide in the next decade due to climatic change. As far as quality and reliability are concerned, DGs give better power because of their location being near consumers [1]. In other words, microgrid (MG) forms a cluster of DGs, with controllers, energy storages, and loads [2]. Controllable DGs also ensure responsible power production and consumption. This regime can maintain the reliability of the network and solve a series of problems caused by large-scale DG access; thus, it becomes an advanced scheme for future power supply and an essential part of smart grid construction [3].

The supply/demand inside MGs working in grid-connected mode gives/draws power. Microgrids work as an independent power system, i.e., at the point when not connected to the main grid is said to be in islanded mode [4]. It is well known that stability plays a crucial role in the quality and reliability of MGs. As per the nature of the disturbance, the MG stability issues can be isolated into small-signal stability and the high disturbance stability [5], [6]. Research on the mathematical model of MG stability analysis and stability improvement methods for the MG is predominantly focused [7], [8]. One of the essential worries among different kinds of stability problems in the MG is the small-signal stability issues [9], [10]. With the end goal to keep up power quality inside the directed range and improve the dynamic performance, it is fundamental to dissect the small-signal model and select diverse parameters for the controller or filter [11], [12]. In the conventional power system, the stability analysis is set up well with the dynamics of the network. Also, in MGs, a small-signal dynamic equation for MGs modeling might be troublesome due to the control strategy of DG on account of complexity and diversity [13]. Thus, modeling and performance analysis of small-signal for MG has bit by bit turned out to be one of the concerning issues [14], [15]. For the small-signal stability, the impacts of droop control gains, line impedance, and load fluctuations on the qualities of MG voltage and frequency are discussed in the ongoing works [16]. In any case, it just acquired the parameters variation for regular pattern and did not advance a particular optimization scheme [17]. For the droop controllers of inverter-interfaced DGs by dynamic model, the particle swarm optimization algorithms

Manuscript received March 7, 2020; revised June 24, 2020; accepted August 10, 2020. This work was supported by the Renewable Energy Lab, College of Engineering, Prince Sultan University, Riyadh, Saudi Arabia. *(Corresponding author: Mahajan Sagar Bhaskar.)*

Anantha Krishnan Venkatesan and O. V. Gnana Swathika are with the School of Electrical Engineering, Vellore Institute of Technology, Chennai 600217, India (e-mail: ananthakrishnan.v@vit.ac.in; gnanaswathika.ov@vit.ac.in).

Umashankar Subramaniam, Mahajan Sagar Bhaskar, and Dhafer J. Almakhles are with the Renewable Energy Lab, Department of Communications and Networks Engineering, College of Engineering, Prince Sultan University, Riyadh 11586, Saudi Arabia (e-mail: shankarums@gmail.com; sagar25.mahajan@gmail.com; dalmakhles@psu.edu.sa).

Sanjeevikumar Padmanaban is with the Department of Energy Techonolgy, Aalborg University, Esbjerg 9220, Denmark (e-mail: san@et.aau.dk).

Massimo Mitolo is with the School of Integrated Design, Engieering and Automation, Irvine Valley College, Irvine, CA 92612 USA (e-mail: mmitolo@ivc.edu).

Digital Object Identifier 10.1109/JSYST.2020.3020509

were utilized. Yet, it just considered the PI controller parameters affect, hence results were not extensive and still further change is required [18]. The MG control strategies have their very own small-signal model to encapsulate the dynamic and steady-state performance [19]. The reference model droop gains are managed at the secondary level by interactive droop management scheme along the ac power flow supervisory control strategy to obtain the nominal setting of the central controller in MG [20]. This article presents the small-signal stability analysis of a distributed generation unit in an autonomous MG operation. The purpose of the proposed strategy is to optimally improve the capacity of the power system to restore the reasonable operating condition following a small physical disturbance. The proposed strategy is the joined execution of both the modified ant-lion optimization algorithm (MALO) and artificial neural network (ANN), and hence it is named as MALANN. The behavior of the inner model-based current and voltage controllers, a state-space model by utilizing small-signal analysis is discussed [21]. In three MG structures, a combination of different DG units was considered to investigate the small-signal stability and possible interaction between sensitive modes, particularly in an autonomous mode of MG operation. For enhancing the performance of the robust controller, robust decentralized servo-mechanism control scheme for autonomous voltage sourced converter-based MGs including multiple distributed energy resources is presented [22]. By a fuzzy logic controller, the presented control scheme adds a new control loop to control the reactive power reference to have the benefit of increasing the system stability margins. Moreover, fitness comparison, robustness and time delay analysis were analyzed.

The review of the recent research work shows that the system stability in the MG is an essential contributing factor in the power distribution system. Small-signal stability is one of the vital problems in the reliable operation of a MG. In such a manner, a few issues regarding the resiliency of MG are concerned, for example, fault ride-through capability, nonlinear and unbalanced loads inclusion, communication time-delay, power-sharing, and advanced MG power-flow techniques. Droop control method utilizes small-signal modeling.

In any case, when load dynamics are considered, it has a weak transient performance and lack of black start capacity. Centralized control demands high-bandwidth communication and thus, failure in communication system lead to system collapse. No solution has been introduced to keep up the stability of the system in large-signal disturbances and the desired power sharing. To overcome these difficulties, optimal detecting using advanced technology is required. In related works, few control systems are introduced to tackle the small-signal disturbances, and the previously mentioned confinements have motivated to do this research work.

The rest of this article is organized as follows. Section II depicts the small-signal stability model of autonomous MG operation. Analysis of small-signal stability for MG using the proposed method is clarified in Section III. Section IV clears up the comparative investigation and appraisal. Finally, Section V concludes this article.

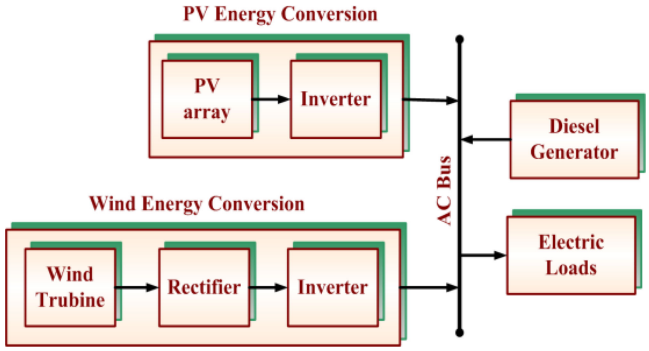

Fig. 1. Typical configuration of microgrid.

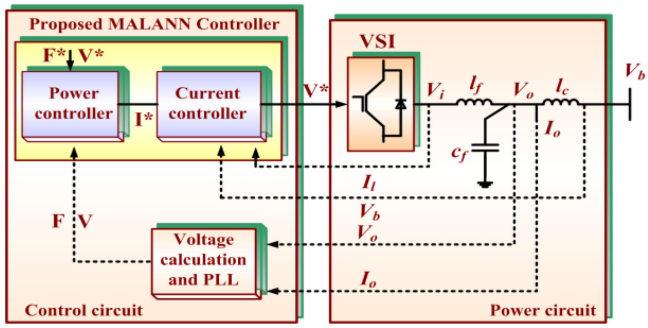

Fig. 2. Schematic diagram of the controlled VSI system.

II. Small-Signal Model of Autonomous Microgrid Operation

In this section, the small-signal stability model of autonomous MG operation is portrayed. A MG setup is portrayed in Fig. 1. In view of their own reference frame *d–q*, these dynamics are depicted. The analysis of the microgrid is considered in a common reference frame *D–Q* and all the sub-models is referred to [6]. Using the accompanying transformation procedure, the output signals of the inverter can be changed over into a common reference frame *D–Q* given by the following:

$$[F_{DQ}] = [T_i][F_{DQi}] \tag{1}$$

where T_i. denotes the transfer matrix of the *i*th DG such that

$$[T_i] = \begin{bmatrix} \cos(\theta_i) & -\sin(\theta_i) \\ \sin(\theta_i) & \cos(\theta_i) \end{bmatrix} \tag{2}$$

where θ_i represents the difference in angles between the reference frame and the *i*th frame. If all the DG resources are voltage source inverter (VSI)-based, then one of them must be regarded as the reference, with its θ being 0 in a MG.

A. State-Space Model of a 3ϕ VSI System

In this section, the model of state-space 3ϕ VSI system and the schematic chart of the controlled VSI system are depicted in Fig. 2. Here, two main circuits can be isolated. The primary power circuit combines the inverter and the output *LC* filter. The second main power circuit comprises the power controller and

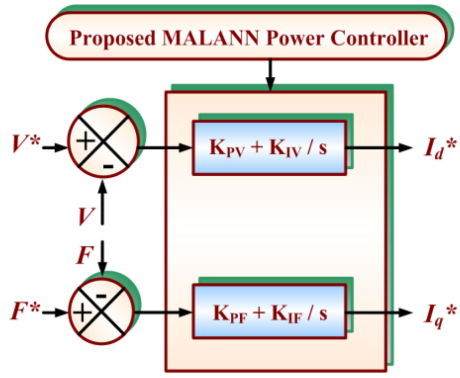

Fig. 3. Block diagram of the proposed MALANN power controller.

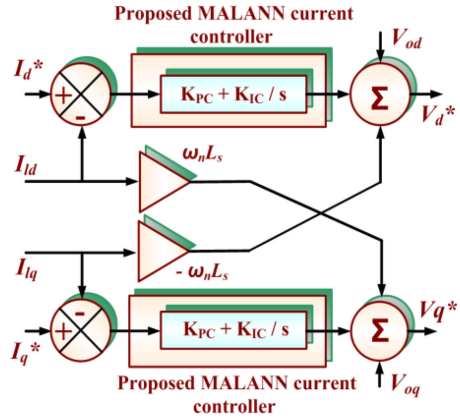

Fig. 4. Block diagram of the proposed MALANN current controller.

current controller. The dynamic of the dc-bus can be disregarded while accepting that the DG unit, which is a constant dc source. Also, because the inverter is a switch-mode device with the sufficiently high switching frequency, the switching action does not affect the states when an excellent attenuation of the switching frequency ripple is achieved through the output *LC* filter [24]. The rest of the parts of the state-space model are depicted as follows.

1) Power Controller: The block diagram of the proposed power controller is shown in Fig. 3. By using the proposed MALANN approach, the system voltage and frequency are directed with a standard PI controller to generate the current reference vectors. The corresponding state-space equations are formulated as follows:

$$\frac{d\xi_d}{dt} = V^* - V, \frac{d\xi_q}{dt} = F^* - F. \tag{3}$$

The output equation is considered from Figs. 3 and 4, and stated as follows:

$$I_d^* = K_{PV}(V^* - V) + K_{IV}\xi_d \tag{4}$$

$$I_q^* = K_{PF}(F^* - F) + K_{IF}\xi_q \tag{5}$$

where I_d^* and I_q^* denote the current reference vectors. Since the power controller input is divided into two terms: reference and the feedback inputs, the state-space equations of a linearized small-signal model can be written as follows:

$$[\Delta\dot{\xi}_{dq}] = a_P[\Delta\xi_{dq}] + b_{P1}[\Delta V^{\bullet}\Delta F^*]^T + b_{P2}[\Delta V \Delta F]^T \tag{6}$$

where

$$\left.\begin{aligned} &\Delta\xi_{dq} = [\Delta\xi_d\ \Delta\xi_q]^T, a_P = [0], b_{P1} = \begin{bmatrix} 1 & 0 \\ 0 & 1 \end{bmatrix}, \\ &b_{P2} = \begin{bmatrix} -1 & 0 \\ 0 & -1 \end{bmatrix} \\ &[\Delta I_{dq}^*] = c_P[\Delta\xi_{dq}] + d_{P1}[\Delta V^*\Delta F^*]^T + d_{P2}[\Delta V\ \Delta F]^T, \\ &\Delta I_{dq}^* = [\Delta I_d^*\ \Delta I_q^*]^T \\ &c_P = \begin{bmatrix} K_{IV} & 0 \\ 0 & K_{IF} \end{bmatrix}, d_{P1} = \begin{bmatrix} K_{PV} & 0 \\ 0 & K_{PF} \end{bmatrix}, \\ &d_{P2} = \begin{bmatrix} -K_{PV} & 0 \\ 0 & -K_{PF} \end{bmatrix} \end{aligned}\right\}. \tag{7}$$

2) Current Controller: The block diagram of the current controller is depicted in Fig. 4. Two PI regulators are used to enhance the steady-state and dynamic performance by eliminating the current error in both the inverter current loop and the grid voltage feed-forward loop. Here, the coupling inductance is not considered, that means, $V_b = V_o$ and the state-space equations can be formulated as follows:

$$\frac{d\delta_d}{dt} = I_d^* - I_{ld}, \frac{d\delta_q}{dt} = I_q^* - I_{lq}. \tag{8}$$

The output equations are formulated as follows:

$$V_d^* = V_{od} - \omega_n L_s I_{lq} + K_{PC}(I_d^* - I_{ld}) + K_{IC}\delta_d \tag{9}$$

where ω_n is the nominal frequency in radian per second in the MG, direct component of the measured output voltage of the DG unit as V_{od}

$$V_q^* = V_{oq} - \omega_n L_s I_{ld} + K_{PC}(I_q^* - I_{lq}) + K_{IC}\delta_q \tag{10}$$

where V_{oq} is a quadratic component of the measured output voltage of the DG unit. The linearized small-signal state-space equations can be formulated as follows:

$$\begin{bmatrix} \Delta\dot{\delta}_{dq} \end{bmatrix} = a_C[\Delta\delta_{dq}] + b_{C1}[\Delta I_{dq}^*]^T + b_{C2}\begin{bmatrix} \Delta I_{ldq} \\ \Delta V_{odq} \\ \Delta I_{odq} \end{bmatrix} \tag{11}$$

where ΔI_{odq} is the output current and

$$\left.\begin{aligned} &\Delta\delta_{dq} = [\Delta\delta_d\ \Delta\delta_q]^T, a_C = [0], b_{C1} = \begin{bmatrix} 1 & 0 \\ 0 & 1 \end{bmatrix}, \\ &b_{C2} = \begin{bmatrix} -1 & 0 & 0\,0\,0\,0 \\ 0 & -1 & 0\,0\,0\,0 \end{bmatrix} \\ &[\Delta V_{dq}^*] = c_C[\Delta\delta_{dq}] + d_{C1}[\Delta I_{dq}^*]^T + d_{C2}\begin{bmatrix} \Delta I_{ldq} \\ \Delta V_{odq} \\ \Delta I_{odq} \end{bmatrix} \end{aligned}\right\}. \tag{12}$$

3) Coupling Inductance and Output LC *Filter:* The inverter drives perfect tracking ($V_i = V*$) is assumed, and using the coupling inductance promote examination is completed. The small-signal state-space equations of the output *LC* filter and the coupling inductance can be obtained as follows:

$$\frac{dI_{ld}}{dt} = -\frac{r_f}{l_f}I_{ld} + \omega_{Ilq} + \frac{1}{l_f}V_{Id} - \frac{1}{l_f}V_{od} \tag{13}$$

where l_f and c_f are the output filter

$$\frac{dI_{lq}}{dt} = -\frac{r_f}{l_f}I_{lq} + \omega_{Ild} + \frac{1}{l_f}V_{Iq} - \frac{1}{l_f}V_{oq} \tag{14}$$

$$\frac{dV_{od}}{dt} = \omega_{Voq} + \frac{1}{c_f}I_{Id} - \frac{1}{c_f}I_{od} \tag{15}$$

$$\frac{dV_{oq}}{dt} = -\omega_{Vod} + \frac{1}{c_f}I_{Iq} - \frac{1}{c_f}I_{oq} \tag{16}$$

$$\frac{dI_{od}}{dt} = -\frac{r_c}{l_c}I_{od} + \omega_{Ioq} + \frac{1}{l_c}V_{od} - \frac{1}{l_c}V_{bd} \tag{17}$$

where l_c is the coupling inductance, a direct component of the measured output current of the DG unit as I_{od}, a quadratic component of the measured output current of the DG unit as I_{oq}

$$\frac{dI_{od}}{dt} = -\frac{r_c}{l_c}I_{oq} + \omega_{Iod} + \frac{1}{l_c}V_{oq} - \frac{1}{l_c}V_{bq}. \tag{18}$$

In view of the own referenced *d–q* frame and using the transformation system given by (1), the inverter output current must be represented in a standard reference *dq* frame which is determined as follows:

$$[\Delta I_{oDQ}] = [T][\Delta I_{odq}]. \tag{19}$$

Using the inverse transformation method, the bus voltage can be changed over into the inverter reference through *d–q* frame as follows:

$$[\Delta V_{bdq}] = [T]^{-1}[\Delta V_{bDQ}]. \tag{20}$$

The overall state-space model of the inverter can be characterized by combining the state-space equations of the power controller, current controller, and the output *LC* filter given by (6), (7), (11), (12), (18), and (19). The dynamic inverter model can be described by the following:

$$\left[\Delta\dot{X}_{\mathrm{Inv}}\right] = \begin{pmatrix} a_{\mathrm{inv1}}[\Delta X_{\mathrm{Inv}}] + a_{\mathrm{inv2}}[\Delta V^*\Delta F^*]^T \\ +a_{\mathrm{inv3}}[\Delta V\Delta F]^T + b_{\mathrm{inv}}[\Delta V_{bDQ}] \end{pmatrix} \tag{21}$$

$$[\Delta I_{oDQ}] = c_{\mathrm{Inv}}[\Delta X_{\mathrm{Inv}}]. \tag{22}$$

B. State-Space Model of the Network and Load

In this section, the small-signal state-space model of the network and load are discussed. Assuming that there is *L* number of loads and *N* is the number of network nodes, which yields *LN* number of lines; the corresponding state-space equation of the loads can be resolved given the accompanying condition

$$\left[\Delta\dot{I}_{\mathrm{load}DQ}\right] = a_{\mathrm{load}}[\Delta I_{\mathrm{load}DQ}] + b_{\mathrm{load}}[\Delta V_{bDQ}] \tag{23}$$

where $\Delta\dot{I}_{\mathrm{load}DQ}$ represents the *i*th load connected to the *j*th node such that

$$[\Delta I_{\mathrm{load}DQ}] = [\Delta I_{\mathrm{load}DQ1}\ \Delta I_{\mathrm{load}DQ2}\ \ldots\ \Delta I_{\mathrm{load}DQL}]^T.$$

The network state-space equation can be mathematically formulated as follows:

$$[\,\Delta\dot{I}_{\mathrm{line}DQ}] = a_{\mathrm{net}}[\Delta I_{\mathrm{line}DQ}] + b_{\mathrm{net}}[\Delta V_{bDQ}]. \tag{24}$$

TABLE I
PARAMETERS OF THE SYSTEM

Parameters	Value
Number of the converter in	3 (DGs)
DG-1 (PV)	600W
DG-2 (Wind)	276W
DG-3 (Diesel generator set)	400W
Converter Structure	3ϕ H-Bridge Inverter
Converter loss	R=0.1Ω/phase
LC filter	l_f=49.8mH, c_f =50μF
Voltage	415 V
Frequency	50Hz
Grid Impedance	2.5Ω, 20mH
Load	520W

For the network with the *i*th lines in (24), the following equation is derived:

$$[\Delta I_{\mathrm{net}DQ}] = [\Delta I_{\mathrm{net}DQ1}\ \Delta I_{\mathrm{net}DQ2}\ \ldots\ \Delta I_{\mathrm{net}DQLN}]^T.$$

C. Microgrid Overall Model

The complete models of the inverter, network, and load are often combined to represent the overall MG model. The voltage in the node is the input to each model; it very well may be found in the linearized equations given by (20), (22), and (23). Between each network node and ground, there is a virtual resistance (r_N) of significant magnitude in the range ($r_N \leq 1000\ \Omega$) [6]. Load current and the line current the equation for the node voltage can be equated as follows:

$$\Delta V_{bDQi} = rN\left(\Delta I_{oDQi} - \Delta I_{\mathrm{load}DQi} + \Delta I_{\mathrm{net}DQi}\right). \tag{25}$$

The MG model for the node voltage is derived as follows:

$$\Delta V_{bDQi} = R_N\big(m_{\mathrm{Inv}}[\Delta I_{oDQi}] + m_{\mathrm{load}}[\Delta I_{\mathrm{load}DQi}] + m_{\mathrm{net}}[\Delta I_{\mathrm{net}DQi}]\big) \tag{26}$$

where a diagonal matrix of size ($2N \times 2N$) with elements equal to r_N is specified as R_N. A ($2N \times 2L$) matrix with -1 elements are taken for the loads and considered as m_{load}, ($2N \times 2L_N$) matrix with ± 1 element considering the direction of the node current as m_{net}. The overall small-signal state-space model of the MG can be formulated by using the linearized state-space equations (21), (23), and (24) as follows:

$$\begin{bmatrix} \Delta\dot{X}_{\mathrm{Inv}} \\ \Delta I_{\mathrm{line}DQ} \\ \Delta I_{\mathrm{load}DQ} \end{bmatrix} = a_{MG} \begin{bmatrix} \Delta X_{\mathrm{Inv}} \\ \Delta I_{\mathrm{line}DQ} \\ \Delta I_{\mathrm{load}DQ} \end{bmatrix} \tag{27}$$

where the system state matrix α_{MG} is formulated based on the following equation. Through the matrix α_{MG}, the stability analysis can be investigated, (28) as shown bottom of the next page.

From the ABCD matrix of the system, eigen-value analysis is performed with A-matrix (a_{MG}) to perform stability analysis with three controllers as this is required for small-signal stability analysis. The controller gains [10] are tuned and compared, as shown in Tables II and III (given in Section IV) for stability analysis. Hence, the eigen-value analysis is not computed. Results of fitness comparison of three methods are included to prove the

TABLE II
OPTIMAL GAIN PARAMETERS FOR VDC REGULATOR

V_{dc} Regulator Gain	Base Case	ALO	Proposed
K_p	20	8	7
K_i	800	800	800

TABLE III
OPTIMAL GAIN PARAMETERS FOR CURRENT REGULATOR

Current Regulator gain	Base case	ALO	Proposed
K_P	0.3	0.5	0.4
K_I	20	21	26

effectiveness of the proposed system

$$\Delta\dot{x} = A_c\Delta x_{\text{conv}} + B_c\Delta v_{tdq} \tag{29}$$

$$\Delta x_{\text{conv}} = [\Delta\delta\Delta P\Delta Q\Delta G_v\Delta G_I\Delta i_{td}\Delta i_{tq} \Delta i_o d\Delta i_o q\Delta v_{cfd}\Delta v_{cfq}]^T. \tag{30}$$

III. PROPOSED METHODOLOGY-BASED SMALL-SIGNAL STABILITY ANALYSIS FOR MICROGRID

In this section, the analysis of small-signal stability for MG using the proposed method is described. The proposed controller is the combination of both the MALO and ANN, named as MALANN. The proposed technique optimally predicts the control parameters of the inner current control loop and the outer power control loop. By using the accomplished dataset of MALO, the ANN is trained, and convincing estimate execution is brought out through the entire machine working condition. For identifying the validity of the controller design, the sensitivity to the control parameters is also presented. The steps for generating the dataset of PI gain parameters using MALO technique have been briefly clarified in the following section.

A. Dataset Generation of PI Gain Parameters Using MALO Algorithm

The ALO algorithm is a population-based arbitrary inquiry technique. It is propelled by the hunting of ants and other prey by the ant lions found in nature [23]. In the ALO algorithm, ants are considered as specialists over the pursuit space which meanders. In the ground, to expand and trap, the ants and ant lions dig pits. By characterizing operations for the ALO technique with the ant and ant lion, the diverse advances, taken amid hunting are modeled. Here, the looking conduct of the ALO technique is balanced by using the capable neighborhood looks for limits like crossover and mutation. In this article, the MALO algorithm is implemented to optimize the control parameters of the inner current control loop, and the outer power control loop in the VSI controlled system.

The MALO algorithm is performed as the global search optimization, and the progression method of the proposed algorithm is considered from the random walk of ants as given below.

1) Random Walks Creation of Ants: The random walks of the ant are created using the following equation:

$$R(t) = \{0, cs(2r(a_{1,}-1), cs(2r(a_{2,})-1), \ldots .cs(2r(a_{l,}-1)\} \tag{31}$$

where the cumulative sum is represented as *cs*, the maximum number of iterations is represented as *l*, and a step of the arbitrary walk is indicated as a stochastic function *r(n),* which is represented as follows:

$$r(n) = \begin{cases} 1 \text{ if random} > 0.5 \\ 0 \text{ if random} \le 0.5. \end{cases} \tag{32}$$

For keeping the random walks as normalized within the search space, the equation is formulated as follows:

$$R_i^t = \frac{(R_i^t - \gamma_i)\ (\kappa_i - \lambda_i^t)}{(\mu_i^t - \gamma_i)} + \lambda_i^t \tag{33}$$

where a minimum of an arbitrary walk of an *i*th variable represented as γ_i, maximum of an *i*th variable at the *t*th iteration is represented as κ_i, minimum of the *i*th variable at the *t*th iteration is indicated asλ_i^t, and the maximum of random walk in the *i*th variable is indicated as μ_i^t. Once the process mentioned above is completed, the MALO-based ANN technique is used to predict the best possible control parameters of the inner current and outer current control loop. The dataset generation flowchart of the MALO algorithm is shown in Fig. 5.

B. Prediction of Optimal PI Gain Parameters Using ANN Technique

The ANN procedure is trained to optimize the PI gain parameters, reference and actual values of voltage, current, and frequency are taken as the network input, and the optimal control parameters are the output of the network. ANN is used to capture the optimal PI gain parameters.

The ANN is trained to compute the reference voltage required for modulation signal. The actual behavior of the system constraints is generating the training data. The learning task is given in the form of the training set. Backpropagation (BP) training algorithm [25] and Levenberg Marquardt algorithm [26] are used in the network to train the dataset. The feed-forward network is trained by the BP algorithm to train the ANN controller to get the optimum and best result. Once the procedure is finished, the ANN is set up to produce the optimal control parameters of the inner current control loop and the outer power control loop. The prediction procedure of the ANN strategy flowchart is depicted in Fig. 6. The proposed strategy is experienced underneath the MATLAB/Simulink stage, and the proficiency of the proposed method is compared with the existing method.

$$a_{\text{MG}} = \begin{bmatrix} a_{\text{Inv}} + b_{\text{Inv}}R_N m_{\text{Inv}} c_{\text{Inv}} & b_{\text{Inv}}R_N m_{\text{Inv}} c_{\text{Inv}} \cdots & \cdots b_{\text{Inv}}R_N m_{\text{load}} \\ b_{\text{net}}R_N m_{\text{net}} c_{\text{net}} & a_{\text{net}} + b_{\text{net}}R_N m_{\text{net}} \cdots & \cdots b_{\text{net}}R_N m_{\text{load}} \\ b_{\text{load}}R_N m_{\text{inv}} c_{\text{inv}} & b_{\text{load}}R_N m_{\text{net}} \cdots & \cdots a_{\text{load}} + b_{\text{load}}R_N m_{\text{load}} \end{bmatrix} \tag{28}$$

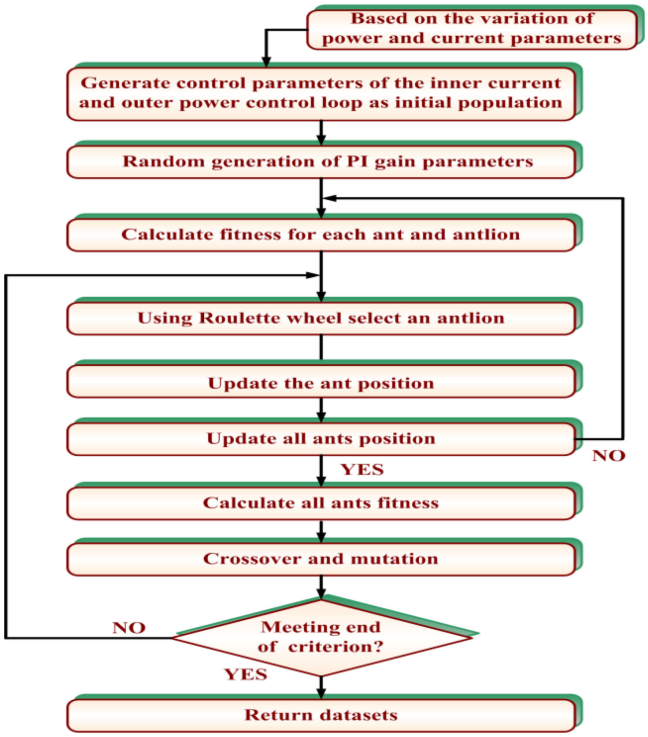

Fig. 5. Generation of the dataset using MALO algorithm.

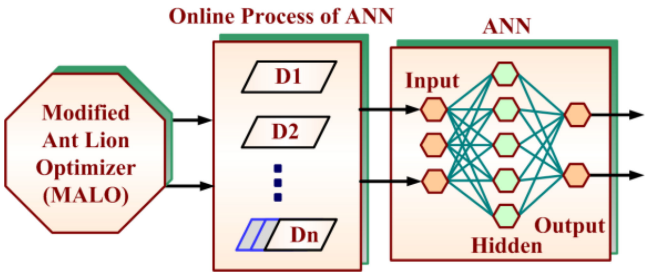

Fig. 6. Prediction procedure of ANN strategy.

IV. Results and Discussion

In this section, the proposed method is compared with the existing techniques and implemented in the MATLAB/simulation working stage to show the effectiveness of the proposed approach effectiveness. By utilizing the proposed technique, the gain parameters of the PI controller are tuned optimally, and the controller offers a reliable system operation. The proposed system is tested based on two test cases such as irradiance change and the load change from 0.6 to 0.8 time period, and their results are compared with different solution techniques such as base and ALO. The proposed approach for two test cases is discussed below. The parameters of the system are tabulated in Table I. The controller values depend on the error of I_d and I_d in the iterative function. For each iteration, the values are taken by the equation modeling

$$u(i) = k_p \times \text{err\_}i_d(i) + ki \times \text{err\_}i_d(i). \quad (34)$$

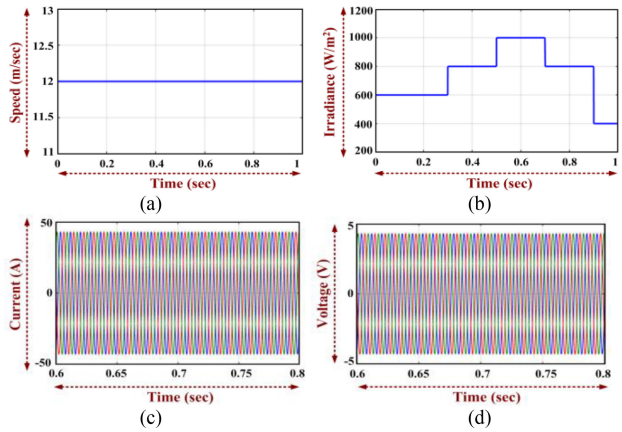

Fig. 7. Simulation waveforms for test case 1 (wind). (a) Wind Speed. (b) Irradiance. (c) Current using the proposed method. (d) Voltage using the proposed method.

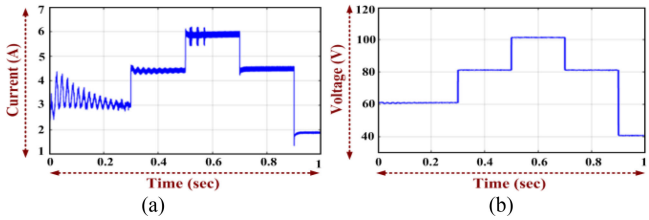

Fig. 8. Simulation waveforms for test case 1 (PV). (a) Current using the proposed method. (b) Voltage using the proposed method.

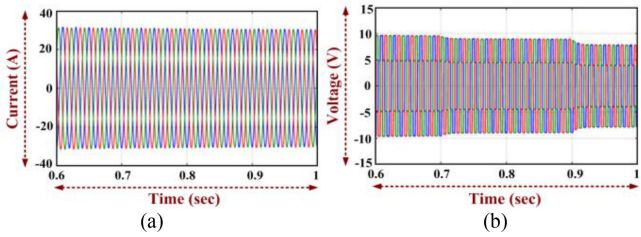

Fig. 9. Simulation waveforms for test case 1 (Diesel Generator). (a) Current using the proposed method. (b) Voltage using the proposed method.

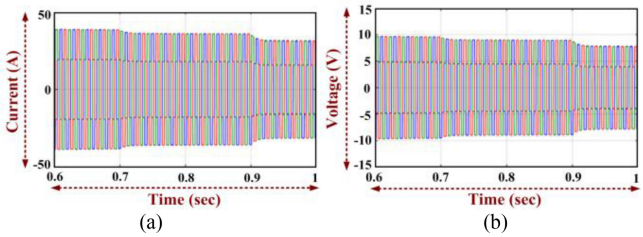

Fig. 10. Simulation waveforms for test case 1 (Load). (a) Current using the proposed method. (b) Voltage using the proposed method.

Finally, the best solution value is taken for the controller. The optimal controller tuning values are given in Tables II and III.

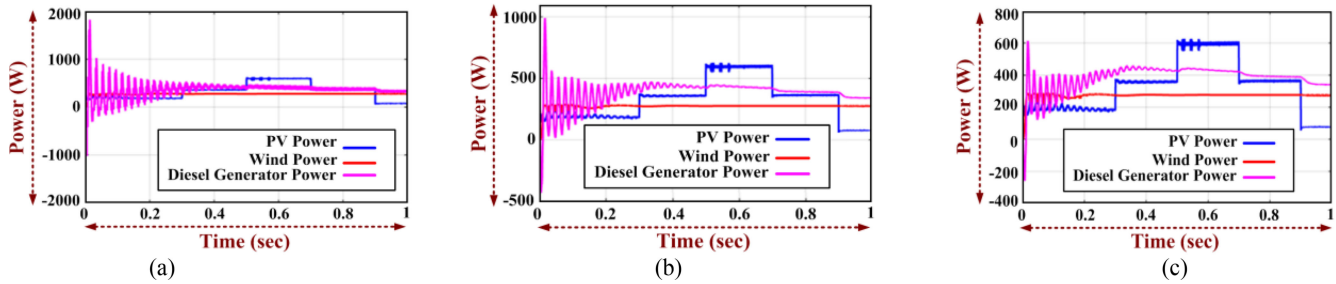

Fig. 11. Individual power comparison of proposed scheme with various existing technique. (a) Base method. (b) ALO. (c) Proposed MALANN.

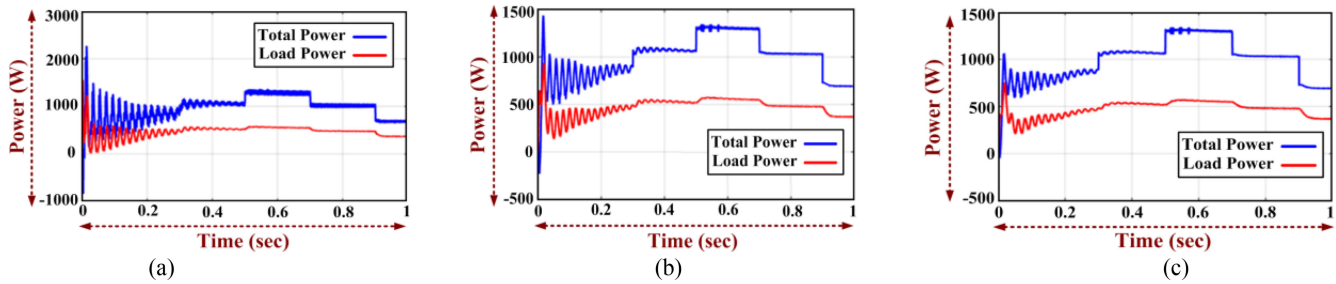

Fig. 12. Total power and load power comparison. (a) Base method. (b) ALO. (c) Proposed MALANN.

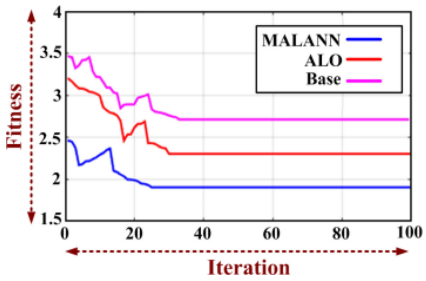

Fig. 13. Fitness comparison of the proposed method with existing techniques.

A. Test Case 1: Irradiance Change

In this section, the change in the irradiance for test case 1 is studied. Fig. 7 shows the analysis of wind speed and irradiation in test case 1. As seen in Fig. 7(a), the wind speed (m/s) in this condition is set as constant. Fig. 7(b) shows the irradiance changes concerning time. The irradiance (W/m^2) initially starts at 600 W/m^2, and the variation happens at time $t = 0.25$ to 1 s, which reaches the irradiance of 400 W/m^2. Fig. 7(c) and (d) show the wind current and wind voltage using the proposed technique, respectively.

In the irradiance change condition, the wind current and voltage are considered at a reasonable condition. Fig. 8 shows the analysis of PV current and PV voltage using the proposed technique under irradiance change. In Fig. 8(a), the PV current varies at time $t = 0.25$–1 s, and the corresponding PV current varies due to the irradiance change from 2.5 to 1.9 A. Fig. 8(b) shows that the PV voltage varies at time $t = 0.25$–1 s and the corresponding PV voltage varies due to the irradiance change from 61 to 39 V. The analysis of diesel generator current and voltage using the proposed technique under irradiance change is plotted in Fig. 9. Fig. 9(a) depicts that the diesel generator current under irradiance change consistently manages the system to reasonable condition with the current of 30 A. In contrast, the diesel generator voltage under irradiance change gradually varies at time $t = 0.69$–1 s, and the voltage reaches 8V. The analysis of load current and load voltage using the proposed method in test case 1 is plotted in Fig. 10. From Fig. 10(a), the load current varies at time $t = 0.69$–1 s when the corresponding load current reaches 40 A. From Fig. 10(b), the load voltage varies at time $t = 0.69$–1 s when the corresponding load voltage reaches 8 V.

The individual power comparison of the proposed strategy with various existing technologies such as base and ALO methods is portrayed in Fig. 11. As shown in the base method in Fig. 11(a), the PV, wind, and diesel generator give less amount of power compared with ALO and proposed technique. The PV power for base method produces 500 W. For the base method, wind power is varied, and after some time, wind power produces a constant power. Initially, the diesel generator power attains 1800 W which slightly decrease to 200 W.

In Fig. 11(b), the individual power comparison using the ALO method is depicted. It shows that PV power produces 520 W. Wind power produces the constant power of 300 W with slight variation. The diesel generator power attains the power of 1000 W, and the power decreases to 400 W. Fig. 11(c) portrays the PV power using the proposed method. Under irradiation change, the PV power slightly varied to produce a power of 600 W. The wind power produces a constant output of 310 W. The diesel generator power of the proposed method reaches

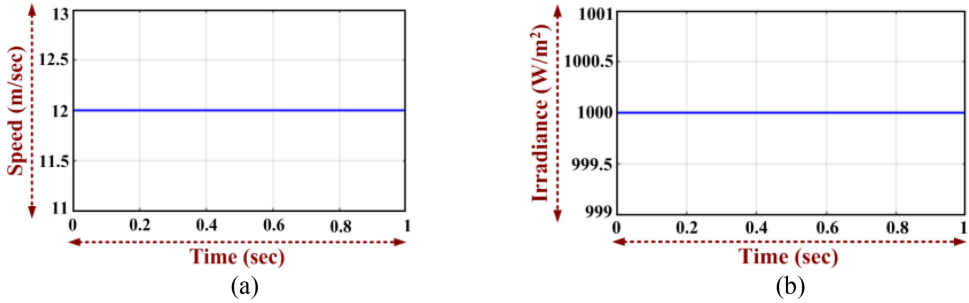

Fig. 14. Simulation waveforms for test case 2 (wind). (a) Wind Speed. (b) Irradiance.

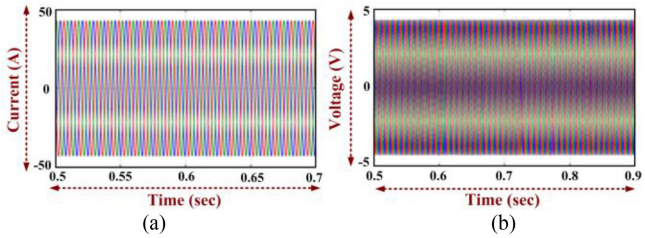

Fig. 15. Simulation waveforms for test case 2 (wind). (a) Current using the proposed method. (b) Voltage using the proposed method.

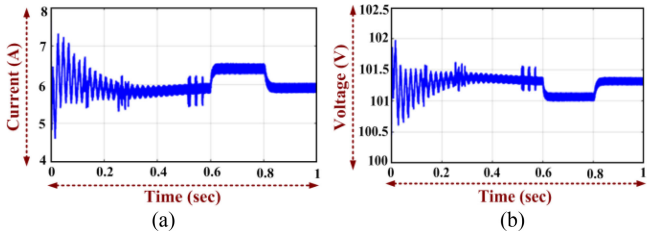

Fig. 16. Simulation waveforms for test case 2 (PV). (a) Current using the proposed method. (b) Voltage using the proposed method.

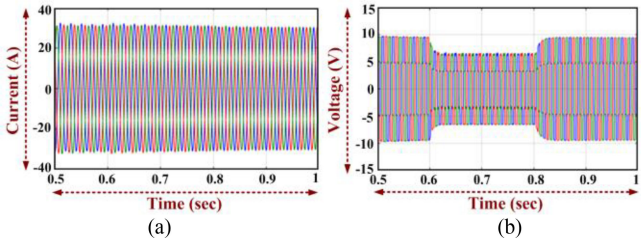

Fig. 17. Simulation waveforms for test case 2 (Diesel Generator). (a) Current using the proposed method. (b) Voltage using the proposed method.

from 600 to 380 W due to the irradiance change condition. Fig. 12 shows the comparison of total power and load power of proposed method with existing techniques. In the base method, Fig. 12(a) depicts that during irradiance change condition, the total power initially starts at 2000 W and decreases to 800 W. The load power ranges from 1500 to 500 W during the irradiance change condition. By using the ALO method, Fig. 12(b) depicts that the total power is initially under 1400 W and decreases to 700 W. The load power ranges 900–400 W in the irradiation change case. Fig. 12(c) shows the total power and load power production using the proposed method analyses. The total power reaches a maximum power of 1400 W and the load power initially in the maximum power of 800–410 W. Fig. 13 shows the comparison of fitness plot of the proposed method with the existing technique under irradiance change condition. As seen in Fig. 13, the proposed method gives an optimal solution when compared with the existing technique.

B. Test Case 2: Load Change

In this test case, the load change condition under the period of 0.6–0.8 s, the system is investigated. Fig. 14 shows the analysis of wind speed and irradiance. Under the load changing condition, the wind speed is constant with a speed of 12 m/s. In the irradiance under load changing condition, the irradiance is 1000 W/m^2. Fig. 15 shows the analysis of wind current and wind voltage under varying load condition. As seen in Fig. 15(a) and (b), the wind current produces a constant current, and the wind voltage produces a constant voltage due to the load changing condition. Fig. 16 shows the analysis of PV current and PV voltage using the proposed method under the load changing condition.

In Fig. 16(a) the PV current changes from 7.5 to 6 A due to the load change condition in the system. In Fig. 16(b), the PV voltage changed from 102 to 101.3 V due to the load change condition. Fig. 17 shows the analysis of diesel generator current and voltage using a proposed method in test case 2. The diesel generator current under load change condition produces a constant amount of current as shown in Fig. 17(a). Fig. 17(b) shows the diesel generator voltage under load change condition, it attains a deviation at time $t = 0.6$ to 0.8 s, the diesel generator current produces 7 V. The analysis of load current and voltage using the proposed method under load change condition is shown in Fig. 18. In Fig. 18(a), the load current deviates from 0.6 to 0.8 s and produces 40 A of load current. Fig. 18(b) shows the load voltage using the proposed method under load change conditions, the deviation happens at 0.6–0.8 s with 8 V of load voltage. The individual power comparison of the proposed method with various existing technologies such as base and ALO method is portrayed in Fig. 19. By using the base method in Fig. 19(a), the PV, wind and diesel generator power gives less amount of power compared with ALO and proposed technique.

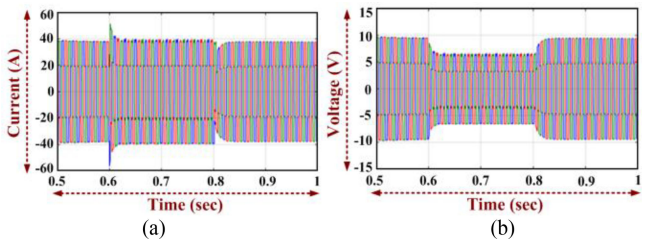

Fig. 18. Simulation waveforms for test case 2 (Load). (a) Current using proposed method. (b) Voltage using proposed method.

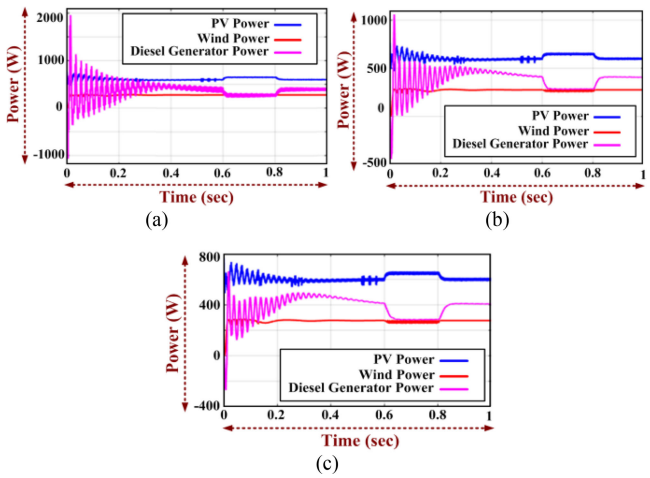

Fig. 19. Individual power comparison of proposed scheme with various existing techniques. (a) Base method. (b) ALO. (c) Proposed MALANN.

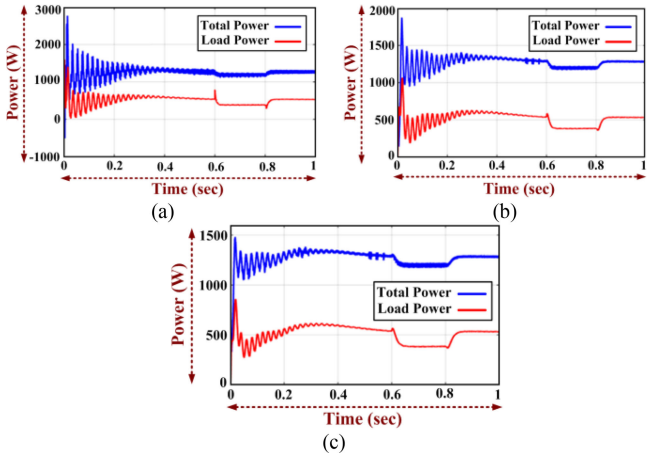

Fig. 20. Total power and load power comparison. (a) Base method. (b) ALO. (c) Proposed MALANN.

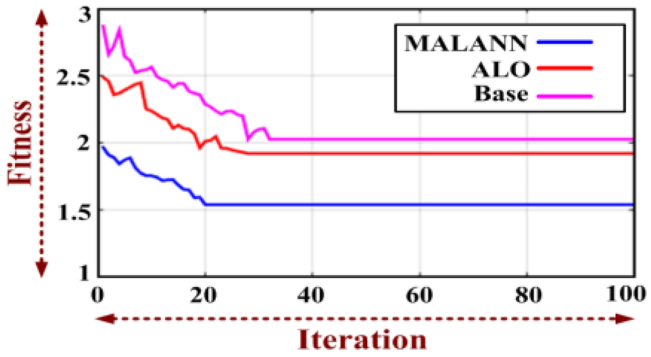

Fig. 21. Fitness comparison of the proposed method with existing techniques.

The PV power for the base method is 650 W. For the base method, wind power is varied, and after some time, wind power produces constant power. Initially, the diesel generator power attains 1900 W and slightly decreases to 500 W. In Fig. 19(b), the individual power comparison using the ALO method is depicted. It gives the PV power of 620 W. Wind power produces the constant power of 300 W with slight variation. The diesel generator power attains the power of 1100 W, and the power decreases to 450 W. Fig. 19(c) portrays the PV power using the proposed method. The PV power under load change condition slightly varied and produces a power of 750 W. The wind power produces a constant output of 320 W. The diesel generator power of the proposed method reaches 640–400 W due to the load change condition.

Fig. 20 shows the comparison of total power and load power of the proposed method with existing techniques. In the base method, Fig. 20(a) depicts that during load change condition, the total power initially starts at 2800 W and decreases to 1200 W. The load power ranges from 1500 to 500 W during the load change condition. By using the ALO method, Fig. 20(b) depicts that the total power is initially under 1800 W and decreases to 1300 W. The load power ranges 1100–510 W in the load change condition. In Fig. 20(c), the proposed method analyzes the total power and load power production. The total power reaches a maximum power of 1490 W and the load power initially is in the maximum power of 800 W which decreases to 510 W. As shown in Fig. 21, the proposed method gives an optimal solution when compared with the existing technique.

Here, the feedback gains impact on the stability of the system is tested by increasing the gain of the power controller gradually. From the overall analysis, the system produces a stable and reliable operation by utilizing the proposed controller.

V. Conclusion

In this article, a small-signal stability analysis of a distributed generation unit influenced by climatic changes in an autonomous MG operation employing MALANN strategy was proposed. The proposed strategy was utilized for restoring the reasonable operating condition of the MG. The proposed strategy optimally predicted the control parameters of the inner current control loop and the outer power control loop considering a variety of current and power parameters. The proposed controller is actualized in the MATLAB/Simulink platform. The proposed model is used to examine the system stability by using the MALANN controller to evaluate the system operation using the fitness convergence. The small-signal analysis is driven by the linearized system state matrix to investigate the oscillatory system mode and the sensitivity to controller parameters. Subsequently, the proposed strategy is a promising technique for determining complicated

problems and the stability analysis is reasonably accurate, and the controller offers a reliable system's operation.

ACKNOWLEDGMENT

The authors express their gratitude to the Renewable Energy Lab, College of Engineering, Prince Sultan University, Riyadh, Saudi Arabia, for technical support.

REFERENCES

[1] D. Dheer, N. Soni, and S. Doolla, "Improvement of small signal stability margin and transient response in inverter-dominated microgrids," *Sustain. Energy, Grids Netw.*, vol. 5, pp. 135–147, 2016.
[2] K. Yu, Q. Ai, S. Wang, J. Ni, and T. Lv, "Analysis and optimization of droop controller for microgrid system based on small-signal dynamic model," *IEEE Trans. Smart Grid*, vol. 7, no. 2, pp. 695–705, Mar. 2016.
[3] F. Katiraei, M. Iravani, and P. Lehn, "Small-signal dynamic model of a micro-grid including conventional and electronically interfaced distributed resources," *IET Gener., Transmiss. Distrib.*, vol. 1, no. 3, pp. 369–378, 2007.
[4] E. Barklund, N. Pogaku, M. Prodanovic, C. Hernandez-Aramburo, and T. Green, "Energy management in autonomous microgrid using stability-constrained droop control of inverters," *IEEE Trans. Power Electron.*, vol. 23, no. 5, pp. 2346–2352, Sep. 2008.
[5] Y. Mohamed and E. El-Saadany, "Adaptive decentralized droop controller to preserve power sharing stability of paralleled inverters in distributed generation microgrids," *IEEE Trans. Power Electron.*, vol. 23, no. 6, pp. 2806–2816, Nov. 2008.
[6] R. Majumder, B. Chaudhuri, A. Ghosh, R. Majumder, G. Ledwich, and F. Zare, "Improvement of stability and load sharing in an autonomous microgrid using supplementary droop control loop," *IEEE Trans. Power Syst.*, vol. 25, no. 2, pp. 796–808, May 2010.
[7] Z. Zeng, H. Yang, and R. Zhao, "Study on small signal stability of microgrids: A review and a new approach," *Renewable Sustain. Energy Rev.*, vol. 15, no. 9, pp. 4818–4828, 2011.
[8] M. Sanjari and G. Gharehpetian, "Small signal stability based fuzzy potential function proposal for secondary frequency and voltage control of islanded microgrid," *Elect. Power Compon. Syst.*, vol. 41, no. 5, pp. 485–499, 2013.
[9] P. Basak, S. Chowdhury, S. Halder N. Dey, and S. Chowdhury, "A literature review on integration of distributed energy resources in the perspective of control, protection and stability of microgrid," *Renewable Sustain. Energy Rev.*, vol. 16, no. 8, pp. 5545–5556, 2012.
[10] R. Majumder, "Some aspects of stability in microgrids," *IEEE Trans. Power Syst.*, vol. 28, no. 3, pp. 3243–3252, Aug. 2013.
[11] H. Liang, B. Choi, W. Zhuang, and X. Shen, "Stability enhancement of decentralized inverter control through wireless communications in microgrids," *IEEE Trans. Smart Grid*, vol. 4, no. 1, pp. 321–331, Mar. 2013.
[12] S. Iyer, M. Belur, and M. Chandorkar, "A generalized computational method to determine stability of a multi-inverter microgrid," *IEEE Trans. Power Electron.*, vol. 25, no. 9, pp. 2420–2432, Sep. 2010.
[13] S. Mishra and D. Ramasubramanian, "Improving the small signal stability of a PV-DE-dynamic load-based microgrid using an auxiliary signal in the PV control loop," *IEEE Trans. Power Syst.*, vol. 30, no. 1, pp. 166–176, Jan. 2015.
[14] M. Illindala and G. Venkataramanan, "Small signal stability of a microgrid with parallel connected distributed generation," *Intell. Automat. Soft Comput.*, vol. 16, no. 2, pp. 235–254, 2010.
[15] M. Delghavi and A. Yazdani, "An adaptive feed-forward compensation for stability enhancement in droop-controlled inverter-based microgrids," *IEEE Trans. Power Del.*, vol. 26, no. 3, pp. 1764–1773, Jul. 2011.
[16] E. Coelho *et al.*, "Small-signal analysis of the microgrid secondary control considering a communication time delay," *IEEE Trans. Ind. Electron.*, vol. 63, no. 10, pp. 6257–6269, Oct. 2016.
[17] H. Baghaee, G. Gharehpetian, and M. Mirsalim, "Real-time verification of new controller to improve small/large-signal stability and fault ride-through capability of multi-DER microgrids," *IET Gener., Transmiss. Distrib.*, vol. 10, no. 12, pp. 3068–3084, 2016.
[18] S. Liu, P. Liu, and X. Wang, "Stochastic small-signal stability analysis of grid-connected photovoltaic systems," *IEEE Trans. Ind. Electron.*, vol. 63, no. 2, pp. 1027–1038, Feb. 2016.
[19] H. Moussa, A. Shahin, J. Martin, S. Pierfederici, and N. Moubayed, "Optimal angle droop for power sharing enhancement with stability improvement in islanded microgrids," *IEEE Trans. Smart Grid*, vol. 9, no. 5, pp. 5014–5026, Sep. 2018.
[20] Y. Zhang, L. Xie, and Q. Ding, "Interactive control of coupled microgrids for guaranteed system-wide small signal stability," *IEEE Trans. Smart Grid*, vol. 7, no. 2, pp. 1088–1096, Mar. 2016.
[21] S. Leitner, M. Yazdanian, A. Mehrizi-Sani, and A. Muetze, "Small-signal stability analysis of an inverter-based microgrid with internal model–based controllers," *IEEE Trans. Smart Grid*, vol. 9, no. 5, pp. 5393–5402, Sep. 2018.
[22] H. Baghaee, M. Mirsalim, G. Gharehpetian, and H. Talebi, "A generalized descriptor-system robust H∞ control of autonomous microgrids to improve small and large signal stability considering communication delays and load nonlinearities," *Int. J. Elect. Power Energy Syst.*, vol. 92, pp. 63–82, 2017.
[23] P. Saxena and A. Kothari, "Ant lion optimization algorithm to control side lobe level and null depths in linear antenna arrays," *AEU, Int. J. Electron. Commun.*, vol. 70, no. 9, pp. 1339–1349, 2016.
[24] N. Kroutikova, C. A. Hernandez-Aramburo, and T. C. Green, "Statespace model of grid connected inverters under current control mode," *IET Elect. Power Appl.*, vol. 1, no. 3, pp. 329–338, 2007.
[25] S. Nandy, P. P. Sarkar, and A. Das, "Training a feed-forward neural network 498 with artificial bee colony based back propagation method," *Int. J. Comput. Sci. Inf. Technol.*, vol. 4, no. 4, pp. 33–46, 2012.
[26] B. M. Wiliamowski and J. D. Irwin, *The Industrial Electronics Handbook*, vol. 5, 2nd ed. Boca Raton, FL, USA: CRC Press, 2012, ch. 12, pp. 12-1–12-5.

Anantha Krishnan Venkatesan received the B.E. degree in electrical and electronics engineering from Madras University, Chennai, India, 2001, and the M.E. degree in power systems engineering from the College of Engineering, Guindy, Anna University, Chennai, 2006.

He is working as an Assistant Professor with the School of Electrical Engineering, Vellore Institute of Technology, Chennai, India. His current research interests include microgrids, stability analysis in microgrid, neural network, and fuzzy logic controller applications.

Umashankar Subramaniam (Senior Member, IEEE) received the bachelor's degree in electrical and electronics engineering from the Government College of Technology, Coimbatore, India, in 2001, the master's degree in power electronics and the Ph.D. degree in electrical engineering from VIT University, India, in 2004 and 2013, respectively.

He is with the Renewable Energy Lab, College of Engineering, Prince Sultan University, Riyadh, Saudi Arabia, and has 15+ years of teaching, research, and industrial R&D experience. Previously, he worked as an Associate Professor and the Head, VIT Vellore, as well as a Senior R&D and Senior Application Engineer in the field of power electronics, renewable energy and electrical drives.

Mr. Subramaniam is a member of International Association of Computer Science and Information Technology, IDES, and Indian Society for Technical Education. He has been the Vice-Chair - IEEE Madras section and the Chair - IEEE student activities from 2018 to 2019.

Mahajan Sagar Bhaskar (Senior Member, IEEE) received the bachelor's degree in electronics and telecommunication engineering from the University of Mumbai, Mumbai, India in 2011 and master's degree in power electronics and drives from the Vellore Institute of Technology, VIT University, India in 2014, and the Ph.D. degree in electrical and electronic engineering, University of Johannesburg, South Africa in 2019.

Currently, he is with Renewable Energy Lab, Department of Communications and Networks Engineering, College of Engineering, Prince Sultan University, Riyadh, Saudi Arabia. He has authored 100 plus scientific papers particular reference to X.Y. converter family, multilevel DC/DC and DC/AC converter, and high gain converter.

O. V. Gnana Swathika (Senior Member, IEEE) received the B.E. degree in electrical and electronics engineering from Madras University, Chennai, India, in 2000, the M.S. degree in electrical engineering from Wayne State University, Detroit, MI, USA, in 2004, and the Ph.D. degree in electrical engineering from VIT University, Chennai, in 2017.

She has also completed her Postdoc at the University of Moratuwa, Sri Lanka. Her current research interests include microgrid protection and energy management system.

Sanjeevikumar Padmanaban (Senior Member, IEEE) received the bachelor's degree in electrical engineering from the University of Madras, Chennai, India, in 2002, the master's (Hons.) degree in electrical engineering from Pondicherry University, Puducherry, India, in 2006, and the Ph.D. degree in electrical engineering from the University of Bologna, Bologna, Italy, in 2012.

He was an Associate Professor with VIT University from 2012 to 2013. In 2013, he joined the National Institute of Technology, India, as a Faculty Member. In 2014, he was invited as a Visiting Researcher with the Department of Electrical Engineering, Qatar University, Doha, Qatar, funded by the Qatar National Research Foundation (Government of Qatar). He continued his research activities with the Dublin Institute of Technology, Dublin, Ireland, in 2014. Furthermore, he served an Associate Professor with the Department of Electrical and Electronics Engineering, University of Johannesburg, Johannesburg, South Africa, from 2016 to 2018. Since 2018, he has been a Faculty Member with the Department of Energy Technology, Aalborg University, Esbjerg, Denmark. He has authored more than 300 scientific papers.

Dhafer J. Almakhles (Senior Member, IEEE) received the B.E. degree in electrical engineering from the King Fahd University of Petroleum and Minerals, Dhahran, Saudi Arabia, in 2006, and the master's (Hons.) degree in electrical engineering and the Ph.D. degree in electrical and computer engineering from The University of Auckland, Auckland, New Zealand, in 2011 and 2016, respectively.

Since 2016, he has been with Prince Sultan University, Riyadh, Saudi Arabia, where he is currently the Chairman with the Communications and Networks Engineering Department, and the Director of the Science and Technology Unit and Intellectual Property Office. He is the leader of the Renewable Energy Research Team and Laboratory.

Massimo Mitolo (Fellow, IEEE) received the Ph.D. degree in electrical engineering from the University of Napoli "Federico II," Naples, Italy, in 1990.

He is a registered Professional Engineer in the state of California and in Italy. He is currently a Full Professor of Electrical Engineering with Irvine Valley College, Irvine, CA, USA, and a Senior Consultant in the matter of failure analysis and electrical safety with Engineering Systems Inc., ESi, Aurora, IL, USA.

Dr. Mitolo is a Fellow of the Institution of Engineering and Technology (IET) of London.